

Beam-Based Vibration Energy Harvesters Tunable Through Folding

Anup Pydah

Department of Biomedical Engineering and
Mechanics (M/C 0219),
Virginia Polytechnic Institute and
State University,
Blacksburg, VA 24061
e-mail: anpydah@vt.edu

R. C. Batra

Clifton C. Garvin Professor
Honorary Mem. ASME
Department of Biomedical Engineering and
Mechanics (M/C 0219),
Virginia Polytechnic Institute and
State University,
Blacksburg, VA 24061
e-mail: rbatra@vt.edu

We present a novel beam-based vibration energy harvester, and use a structural tailoring concept to tune its natural frequencies. Using a solution of the Euler–Bernoulli beam theory equations, verified with finite element (FE) solutions of shell theory equations, we show that introducing folds or creases along the span of a slender beam, varying the fold angle at a crease, and changing the crease location helps tune the beam natural frequencies to match an external excitation frequency and maximize the energy harvested. For a beam clamped at both ends, the first frequency can be increased by 175% with a single fold. With two folds, selective frequencies can be tuned, leaving others unchanged. The number of folds, their locations, and the fold angles act as tuning parameters that provide high sensitivity and controllability of the frequency response of the harvester. The analytical model can be used to quickly optimize designs with multiple folds for anticipated external frequencies. [DOI: 10.1115/1.4040576]

Keywords: vibrational energy harvesters, folds, creases, passive tuning, structural tailoring

1 Introduction

Vibrational energy harvesters extract electrical energy from ambient vibrations to power stand-alone wireless microelectronic devices [1,2]. These harvesters reduce our dependency on environmentally hazardous chemical batteries and can be used for remote health monitoring of structures and machinery with minimal maintenance costs [3]. They use either electrostatic [4] or electromagnetic [5] or piezoelectric (PZT) [6] transduction mechanisms to convert mechanical energy of ambient vibrations to electrical energy. Irrespective of the conversion technique, the harvester delivers maximum power when its natural frequency closely matches the environmental excitation frequency. Small deviations from this resonance condition may severely reduce the harvester performance and efficiency.

Two primary approaches commonly used to optimize the power output of these harvesters under time-dependent external vibrations [7] are: widening the operational bandwidth of the harvester, and tuning its resonant frequency to match the ambient excitation frequency. Broadband energy harvesting can be accomplished by using either an array of cantilever beams [8], or a tuned auxiliary structure [9], or nonlinear systems [10], and is suitable when the ambient excitation contains multiple frequencies with large amounts of spectral content around the resonant frequencies of the harvester. However, their efficiency is low when only one dominant external frequency is present. For such situations, a harvester with an adjustable resonant frequency is generally more efficient.

Active tuning with either an external mechanism or an active material continuously matches the resonant frequency of the harvester with the external frequency, and passive tuning mechanisms, which operate only intermittently, have been demonstrated. Common mechanical tuning methods involve applying axial preloads [11,12], changing the area moment of inertia of the beam [13], and moving a tip mass back and forth along its span [14]. These techniques require external attachments to facilitate the tuning process which are bulky and are unsuitable for self-tuning applications. Magnetic [15] and electric [16] tuning approaches

have also been proposed but require additional sources of input power and complex circuitry.

Here, we propose a novel structural tailoring concept for a passive beam-based vibration harvester. By introducing simple topological folds or creases in slender beams, we show, using the Euler–Bernoulli beam theory equations, that beam's natural frequencies can be tuned over a wide range by varying fold angles, fold locations, and number of folds. The dynamics of L-shaped [17,18] and Z-shaped [19] beams have been investigated for applications as robotic arms, swing-arm cranes and as morphing wing designs for aircrafts. We follow the mechanics of materials (MoM)-based discrete modeling approach proposed for stiffened plates [20,21] and sandwich panels [22–24]. Results of the analytical formulation agree well with those computed by the finite element (FE) studies using the commercial software ABAQUS/EXPLICIT and modeling beam's deformations with a shell theory.

For a beam clamped at both ends, the first natural frequency doubled by using a single fold with the fold angle, α , varying from 0 to 30 deg, while selective frequencies could be tuned leaving others unchanged, by using two folds. By changing the fold angle in situ for precreased beams, the harvester can match its resonant frequencies with varying external conditions. The analytical formulation can be used for multiple folds and for optimizing harvester designs.

2 Concept and Analytical Formulation

Figure 1 shows a slender beam of length L , width B , and thickness H clamped at both ends, $x=0$ and $x=L$, with n folds ($n=3$ for the sketch in the figure) at $x=\eta_i$ ($i=1, 2, \dots, n$) along the beam length. A crease or a fold is defined as a straight line segment along the width of the beam across which the beam has zeroth-order geometric continuity, i.e., the tangent to the beam centroidal axis is discontinuous at the fold line. The beam subsections abutting each fold are called arms. A beam with n folds is comprised of $(n+1)$ arms with the i th fold flanked by the i th and the $[i+1]$ th arms. The zeroth $[(n+1)]$ fold corresponds to the left (right) edge of the beam. A folding motion by an angle α (positive in the clockwise direction) is a rigid rotation of the adjacent arms about the fold line which changes the dihedral angle between them by α while maintaining a constant in-surface distance

Contributed by the Technical Committee on Vibration and Sound of ASME for publication in the JOURNAL OF VIBRATION AND ACOUSTICS. Manuscript received February 23, 2018; final manuscript received June 5, 2018; published online July 24, 2018. Assoc. Editor: Izhak Bucher.

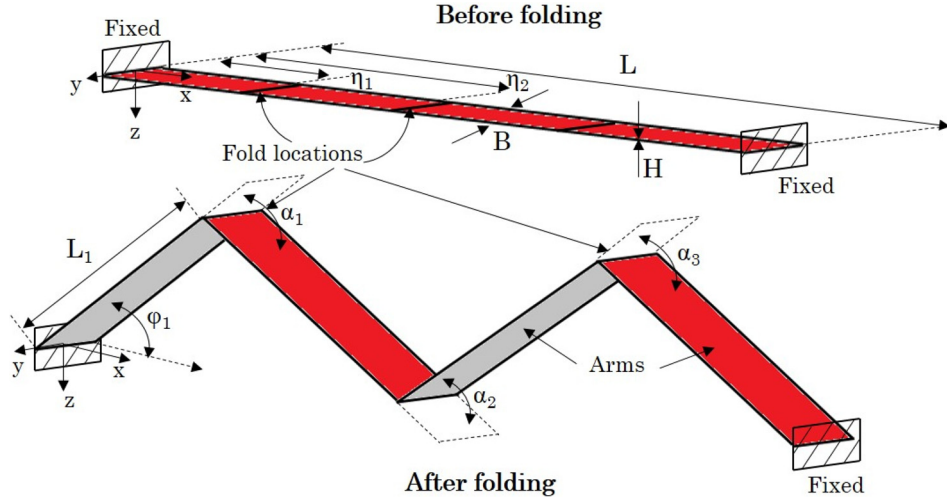


Fig. 1 Schematics of an unfolded beam and of a beam with three folds

between any two points of the beam. Hence, it is assumed that during folding, the deformation is restricted to rotations along the fold line and the length, L_i , of each arm remains constant (see Fig. 2 for rigid folding, by α deg, of a beam with one fold).

In the analytical formulation, the planar deformations (in the xz -plane) of each arm of the beam are modeled *separately* using the kinematic assumptions of the beam theory with the continuity of forces, moments, and displacements enforced at the folds. As shown in Fig. 3 for a candidate arm i of length L_i , two interface forces, $P_i^d(t)$ (along the x -direction; $d=l, r$) and $Q_i^d(t)$ (along the z -direction), and an interface moment $M_i^d(t)$ (about the y -axis) are considered at the left edge (the $(i-1)$ th fold) and at the right edge (the i th fold) of the i th arm. The superscript d takes values l and r to denote, respectively, the left and the right edge of the arm.

In order to facilitate the analysis of deformations of each arm, a local rectangular Cartesian coordinate system (\bar{x}, \bar{z}) is used that is related to the global rectangular Cartesian coordinate axes (x, z) as

$$\begin{Bmatrix} \bar{x} \\ \bar{z} \end{Bmatrix} = \begin{bmatrix} \cos \phi_i & -\sin \phi_i \\ \sin \phi_i & \cos \phi_i \end{bmatrix} \begin{Bmatrix} x \\ z \end{Bmatrix} \quad (1)$$

where ϕ_i ($i=1, 2, \dots, n$) is the inclination angle of the arm, measured counter-clockwise from the positive x -axis as shown in Fig. 1. The transformed interface forces $\bar{P}_i^d(t)$ (along the \bar{x} -direction) and $\bar{Q}_i^d(t)$ (along the \bar{z} -direction), and moment $\bar{M}_i^d(t)$ (about the y -axis) are related to P_i^d , Q_i^d , and M_i^d by

$$\begin{Bmatrix} \bar{P}_i^d \\ \bar{Q}_i^d \end{Bmatrix} = \begin{bmatrix} \cos \phi_i & -\sin \phi_i \\ \sin \phi_i & \cos \phi_i \end{bmatrix} \begin{Bmatrix} P_i^d \\ Q_i^d \end{Bmatrix} \quad (2)$$

$$\bar{M}_i^d = M_i^d$$

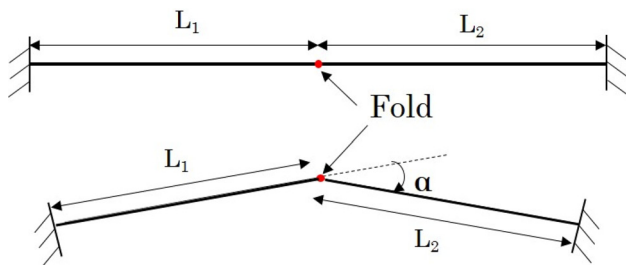


Fig. 2 Rigid folding, by α deg, of an initially flat beam with a single fold ($n=1$). The total length of the beam, $L=L_1+L_2$, remains constant.

Based on assumptions of the EB beam theory, i.e., plane cross sections of the undeformed arm remain plane, undistorted, and normal to the deformed arm axis, and that the beam undergoes free harmonic oscillations with a circular frequency ω , the time-dependent displacement field of the i th arm is given by

$$\begin{aligned} \bar{w}_i(\bar{x}, \bar{z}, t) &= \bar{w}_i^0(\bar{x}) \exp(i\omega t) \\ \bar{u}_i(\bar{x}, \bar{z}, t) &= \left(\bar{u}_i^0(\bar{x}) - \bar{z} \frac{d\bar{w}_i^0}{d\bar{x}} \right) \exp(i\omega t) \end{aligned} \quad (3)$$

where \bar{u}_i^0 and \bar{w}_i^0 are the centroidal displacements of a point of the arm along the \bar{x} - and the \bar{z} -directions, respectively, and t is the time. Ignoring the rotational inertia of the cross section, equations of motion for the arm are

$$\frac{d^2 \bar{u}_i^0}{d\bar{x}^2} + \lambda_u^2 \bar{u}_i^0 = 0 \quad (4)$$

$$\frac{d^4 \bar{w}_i^0}{d\bar{x}^4} - \lambda_w^4 \bar{w}_i^0 = 0 \quad (5)$$

Here, $\lambda_u = \sqrt{\bar{\rho}\omega^2/EA}$, $\lambda_w = (\bar{\rho}\omega^2/EI)^{1/4}$, E is Young's modulus of the beam material, A and I are, respectively, the area and the moment of inertia about the y -axis of the beam cross section, $\bar{\rho}$ is the mass per unit length of the beam and a superimposed dot indicates differentiation with respect to t . In Eqs. (4) and (5), we have assumed that the axial strain, $\varepsilon_{\bar{x}} = (d\bar{u}_i/d\bar{x})$, is infinitesimal, $|\partial^2 \bar{w}_i^0 / \partial \bar{x}^2| \ll 1$, and Hooke's law, $\varepsilon_{\bar{x}} = (\sigma_{\bar{x}}/E)$, holds for the beam material where $\sigma_{\bar{x}}$ is the axial stress.

The solution of Eqs. (4) and (5) is

$$\begin{aligned} \bar{u}_i^0(\bar{x}) &= U_i^1 \cos(\lambda_u \bar{x}) + U_i^2 \sin(\lambda_u \bar{x}) \\ \bar{w}_i^0(\bar{x}) &= W_i^1 \cos(\lambda_w \bar{x}) + W_i^2 \sin(\lambda_w \bar{x}) + W_i^3 \exp(\lambda_w \bar{x}) \\ &\quad + W_i^4 \exp(-\lambda_w \bar{x}) \end{aligned} \quad (6)$$

where the six constants, U_i^1 , U_i^2 , W_i^1 , W_i^2 , W_i^3 , and W_i^4 , can be determined in terms of the unknown interface forces and moments from the boundary conditions

$$\begin{aligned} EA \frac{d\bar{u}_i^0(0)}{d\bar{x}} &= -\bar{P}_i^l, \quad EI \frac{d^3 \bar{w}_i^0(0)}{d\bar{x}^3} = \bar{Q}_i^l, \quad EI \frac{d^2 \bar{w}_i^0(0)}{d\bar{x}^2} = \bar{M}_i^l, \\ EA \frac{d\bar{u}_i^0(L_i)}{d\bar{x}} &= \bar{P}_i^r, \quad EI \frac{d^3 \bar{w}_i^0(L_i)}{d\bar{x}^3} = -\bar{Q}_i^r, \quad \text{and} \quad EI \frac{d^2 \bar{w}_i^0(L_i)}{d\bar{x}^2} = -\bar{M}_i^r \end{aligned} \quad (7)$$

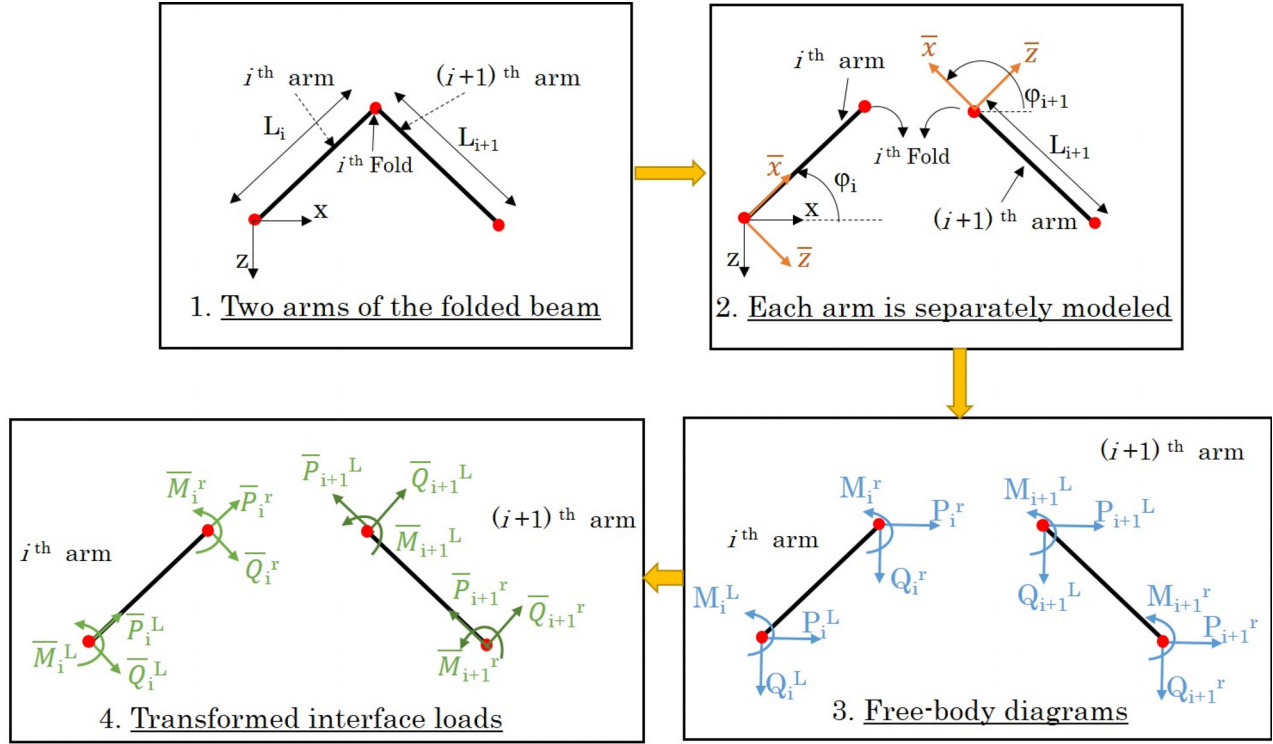


Fig. 3 Interface forces and moments on the i th and the $(i + 1)$ th arms of the folded beam

The displacements $u_i(\bar{x}, \bar{z}, t)$ and $w_i(\bar{x}, \bar{z}, t)$ can then be found in terms of loads P_i^d , Q_i^d and the moment M_i^d by using the transformation rules for vectors.

To ensure continuity of the interface forces and moments as well as of displacements and rotations at the folds, the following six conditions are specified at each fold i , assuming no external loads are applied there

$$\begin{aligned}
 P_i^r + P_{i+1}^l &= 0 \\
 Q_i^r + Q_{i+1}^l &= 0 \\
 M_i^r + M_{i+1}^l &= 0 \\
 w_i(L_i, 0) &= w_{i+1}(0, 0) \\
 u_i(L_i, 0) &= u_{i+1}(0, 0) \\
 \frac{\partial w_i}{\partial x}(L_i, 0) &= \frac{\partial w_{i+1}}{\partial x}(0, 0)
 \end{aligned} \quad (8)$$

The boundary conditions at the clamped left edge of the first arm and the clamped right edge of the $(n + 1)$ th arm are

$$\begin{aligned}
 u_1(0, 0) = w_1(0, 0) &= \frac{\partial w_1}{\partial x}(0, 0) = 0 \\
 u_{n+1}(L_{n+1}, 0) = w_{n+1}(L_{n+1}, 0) &= \frac{\partial w_{n+1}}{\partial x}(L_{n+1}, 0) = 0
 \end{aligned} \quad (9)$$

Imposing continuity conditions (8) and boundary conditions (9) results in an equation for the natural frequencies, ω , of the beam.

It should be noted that other boundary conditions at the beam edges can be easily accommodated.

3 Example Problems

We consider an Aluminum beam with $L = 80$ mm, $B = H = 1$ mm, $\rho = 2700$ kg/m³, $E = 70$ GPa, and $\nu = 0.3$. A fold is introduced at $\eta = 40$ mm creating two arms of equal length, $L_1 = L_2 = 40$ mm. The fold angle α is varied from 0 to 30 deg, which varies the inclination angles of the arms, (ϕ_1, ϕ_2) , from (0,

0) to (15, 165) deg, $\alpha + \phi_2 - \phi_1 = 180$ deg, and the horizontal distance, \bar{L} , of the folded beam between the clamped edges is given by $\bar{L} = L_1 \cos \phi_1 + L_2 \cos \phi_2$. We note that for $\alpha = 0$, the beam is flat and has no folds.

For comparison with the solution of the shell theory equations, we analyzed free vibrations of the clamped folded beam by the finite element method using the commercial software ABAQUS/EXPLICIT [25]. Each arm of the beam is meshed using eight-node shell elements with reduced integration (element S8R) and is discretized into 50 uniform elements along the length and three uniform elements along the width. The FE mesh used was found to give converged natural frequencies within 0.1% tolerance.

Figure 4 shows variation with the fold angle α of the first three nondimensionalized natural frequencies, $\bar{\omega} = \omega(L^2/H)\sqrt{\rho/E}$, of the folded beam as obtained from the MoM or the EB theory formulation and the finite element method using ABAQUS. The nondimensionalization aids in comparing the vibrational frequencies of linearly elastic beams of different dimensions and material properties. Also depicted are the first three mode shapes of the beam, normalized with respect to the value of the peak displacement, as derived from the MoM approach. The maximum difference in the frequencies from the two approaches is 0.66% in $\bar{\omega}_3$ for $\alpha = 26$ deg. Thus, the MoM model accurately determines at least the first three natural frequencies. Results presented in the remaining figures are with the MoM approach.

The gap between the first two nondimensionalized natural frequencies, $\bar{\omega}_2 - \bar{\omega}_1$, reduces from 11.34 for $\alpha = 0$ to 1.23 for $\alpha = 10$ deg, and subsequently increases to 6.1 and 7.2 for $\alpha = 20$ deg and 30 deg, respectively. This could be useful for harvesting energy from rotating machinery or air conditioning equipment where the external excitation has multiple closely spaced frequencies. Most conventional beam-based energy harvesters are designed to match their first resonant frequency with the external frequency, while ignoring higher modes since the spacing between modes is wide. By reducing the gap between specific modal frequencies, our design has the capability to provide broad-band energy harvesting.

For the beam with one fold, the first mode shape for $\alpha = 10$ deg and 20 deg is similar to the second mode shape of the flat beam,

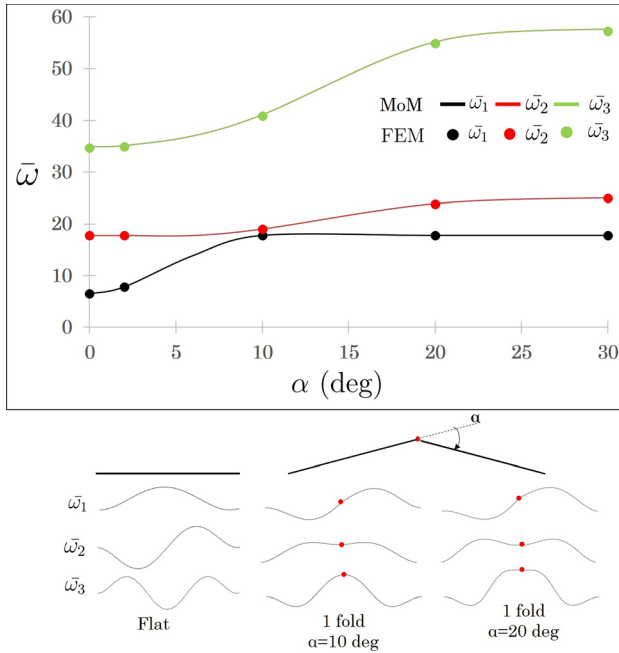


Fig. 4 Variation of the first three nondimensionalized natural frequencies, $\bar{\omega} = \omega(L^2/H)\sqrt{\rho/E}$, and mode shapes with the fold angle α obtained from the FE solution and the MoM formulation for $L_1 = L_2 = 40$ mm

which could explain why the increase in $\bar{\omega}_1$ with the fold angle α saturates as it approaches the value of $\bar{\omega}_2$. However, mode shapes corresponding to $\bar{\omega}_2$ and $\bar{\omega}_3$ are quite different for the folded beam as compared to those for the flat beam. For $\alpha = 10$ deg and 20 deg, the crease locations remain nearly at the beam center, and the mode shapes for the first three frequencies are qualitatively similar to each other.

Figure 5 depicts the percentage change in the first five nondimensionalized frequencies, defined as $(\bar{\omega}_\alpha - \bar{\omega}_0)/\bar{\omega}_0 \times 100$, where $\bar{\omega}_\alpha$ is the frequency for the fold angle α . The first five frequencies correspond to the bending modes of vibration, and their values for the flat beam ($\alpha = 0$) equal 6.46, 17.80, 34.90, 57.68, and 86.19. Increasing the fold angle from 0 to 20 deg increases by 175%, 34%, and 58%, respectively, the first, the second, and the third frequencies, indicating the sensitivity of the frequency to the fold angle. Furthermore, the percentage change in the frequency is not monotonic with the frequency order since the percentage change

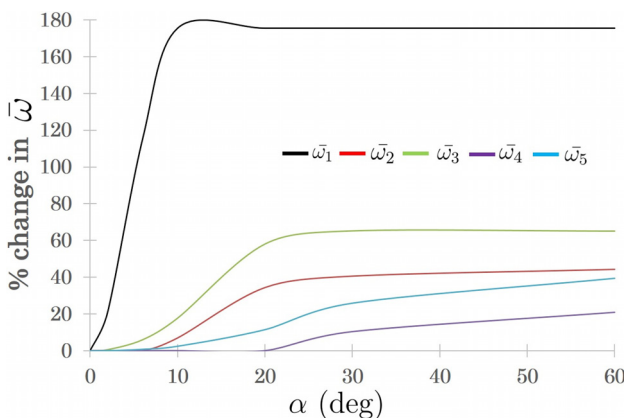


Fig. 5 Percentage change in the first five nondimensionalized frequencies with the fold angle α for $L_1 = L_2 = 40$ mm

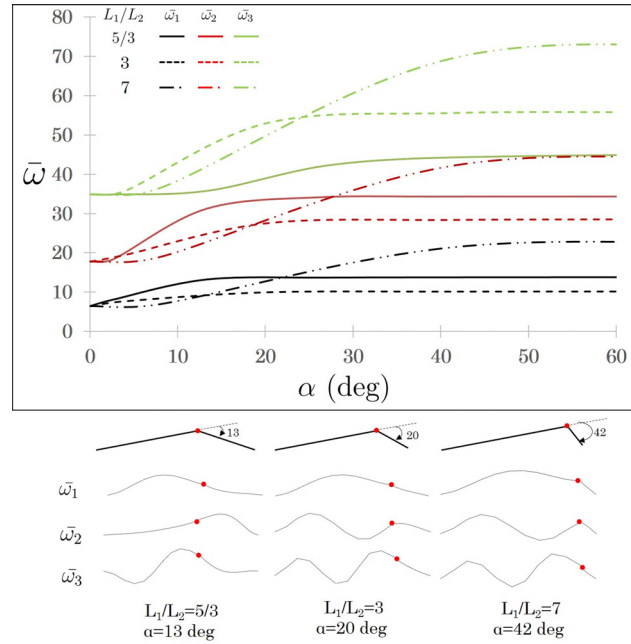


Fig. 6 Effects of changing the location, L_1/L_2 , of the fold on the natural frequencies and mode shapes

in the second frequency is less than that in the first and the third frequencies.

Figure 6 shows effects of changing the location of the fold along the beam span on the first three natural frequencies and mode shapes for $L_1/L_2 = 5/3, 3$, and 7 when the total length of the beam, $L = 80$ mm, is kept constant. Moving the fold from the center of the beam toward the right end with $L_1/L_2 = 7$ and introducing a fold angle $\alpha = 30$ deg can increase $\bar{\omega}_1, \bar{\omega}_2$, and $\bar{\omega}_3$, respectively, by 232%, 140%, and 101%, thereby broadening the tuning range. Thus, the location of the fold can also be varied to tune the natural frequencies. Varying the fold location significantly changes deformations of the beam as depicted by the mode shapes.

For a beam with $L = 60$ mm and $B = H = 1$ mm, Fig. 7 shows effects of increasing the number of folds, from one central fold, $L_1 = L_2 = 30$ mm, to two folds, $L_1 = L_2 = L_3 = 20$ mm, on the first three nondimensionalized natural frequencies. We note that the number of folds and the fold angles can be independently varied; however, results here are depicted only for $|\alpha_1| = |\alpha_2| = \alpha$. For the two-folds' case, results are presented for both, symmetrical folding, $\alpha_1 = \alpha_2 = \alpha$, wherein the sense of the fold angles α_1 and α_2 are the same, and antisymmetrical folding, $\alpha_1 = -\alpha_2 = \alpha$ wherein α_1 and α_2 are of opposite sense. In the two-fold antisymmetrical case, going from an initially flat beam to $\alpha = 30$ deg does not change $\bar{\omega}_1$ but increases $\bar{\omega}_2$ and $\bar{\omega}_3$ by 92% and 32%, respectively, indicating that selective frequencies can be tuned, leaving others unchanged. The results of the symmetrical folding case are consistent with earlier observations of a nonmonotonic increase in frequencies with the fold angle. Thus, increasing the number of folds provides an additional tuning parameter.

Whereas the first mode shape is relatively unaffected in going from one fold to two folds, the second and the third mode shapes are noticeably changed. For the beam with two folds, the second and the third mode shapes for the symmetric ($\alpha_1 = \alpha_2$) and the antisymmetric ($\alpha_1 = -\alpha_2$) cases are quite different.

4 Remarks

The frequencies found in the test cases studied here correspond to the bending mode of vibration primarily because the aspect ratio of each segment, length/thickness, is very large. As shown in

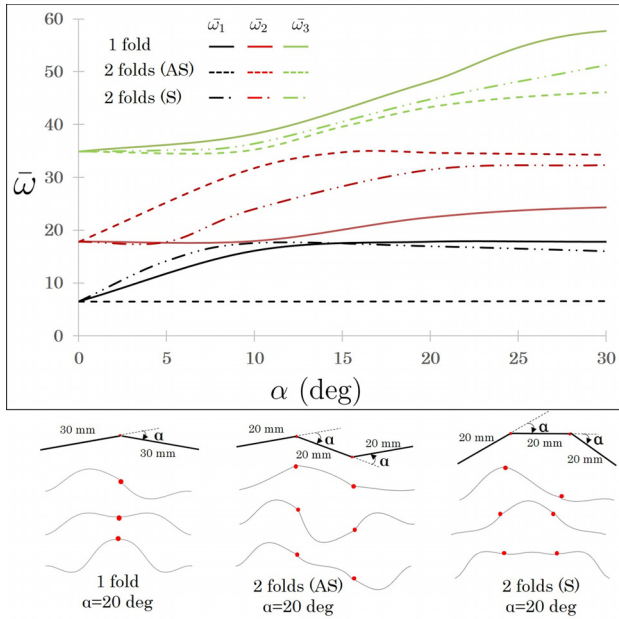


Fig. 7 Effects of increasing the number of folds on the natural frequencies and mode shapes for $L = 60$ mm. In the two fold case, “S” corresponds to symmetrical folding, $\alpha_1 = \alpha_2$, and “AS” to antisymmetrical folding, $\alpha_1 = -\alpha_2$.

Refs. [26–29] for thick beams and plates, the first few frequencies can include the frequency of an in-plane mode of vibration with null deflections or bending.

The energy harvested from a vibrating structure depends not only upon the frequency of vibration but also on the mode shape, the PZT patch shape and location, and the electromechanical coupling coefficients of the PZT material. The location of the PZT determines its deformation modes and their magnitudes. It suggests that for a given PZT material, shape, and size, one should find a combination of frequencies of the tunable harvester, mode shapes, and PZT patch locations to optimize the energy harvested. We will study this optimization problem in the future.

Realizing that energy harvesting is closely related to controlling structural vibrations using PZTs, we note that there is an extensive literature on the latter topic, including some papers by Batra’s group. For example, Batra et al. [30] found that, for the first four modes of vibration, the PZT patches excited with the minimum voltage to control deflections of all points of a simply supported plate should have their centroids at points of the maximum amplitude of initial vibrations of a simply supported plate. Vel and Batra [31] found the polarization direction for the extension-shear bi-morph to be most effective. Ghosh and Batra [32] found, for a plate, the voltage to be applied to the PZT actuators as a function of the surface area covered by them to control plate’s deflections.

5 Conclusions

We have developed a passive tuning strategy for beam-based vibrational energy harvesters wherein the introduction of folds or creases along the beam considerably changes its vibrational frequencies. The location of the folds along the span, the number of folds, and the fold angles provide a diverse space to tune the frequency response of an energy harvester to a wide range of external excitations. We have shown that with a single fold, the first, the second, and the third natural frequencies increase by 175%, 34%, and 58%, respectively, when the fold angle is increased from 0 to 30 deg. The gap between two consecutive natural frequencies can also be tuned to account for external excitations with multiple closely spaced frequencies. Furthermore, in certain fold configurations, selective frequency tuning can be achieved,

wherein only prespecified frequencies are tuned by changing the fold angles. By changing the fold angle for precreased patterns in situ, the harvester can extract the maximum power in environments with varying spectral content. The model developed, results of which have been verified by the FE solutions of shell theory equations, can be used to quickly optimize designs.

Acknowledgment

Views expressed in the paper are those of the authors and neither of ONR nor of Virginia Tech.

Funding Data

- U.S. Office of Naval Research (Grant No. N00014-18-1-2548) to Virginia Polytechnic Institute and State University with Dr. Y. D. S. Rajapakse as the program manager.

References

- [1] Williams, C., and Yates, R. B., 1996, “Analysis of a Micro-Electric Generator for Microsystems,” *Sens. Actuators A*, **52**(1–3), pp. 8–11.
- [2] Cook-Chennault, K., Thambi, N., and Sastry, A., 2008, “Powering MEMS Portable Devices—A Review of Non-Regenerative and Regenerative Power Supply Systems With Special Emphasis on Piezoelectric Energy Harvesting Systems,” *Smart Mater. Struct.*, **17**(4), p. 043001.
- [3] Erturk, A., and Inman, D. J., 2011, *Piezoelectric Energy Harvesting*, Wiley, Hoboken, NJ.
- [4] Mitcheson, P. D., Miao, P., Stark, B. H., Yeatman, E., Holmes, A., and Green, T., 2004, “MEMS Electrostatic Micropower Generator for Low Frequency Operation,” *Sens. Actuators A*, **115**(2–3), pp. 523–529.
- [5] El-Hami, M., Glynne-Jones, P., White, N., Hill, M., Beeby, S., James, E., Brown, A., and Ross, J., 2001, “Design and Fabrication of a New Vibration-Based Electromechanical Power Generator,” *Sens. Actuators A*, **92**(1–3), pp. 335–342.
- [6] Sodano, H. A., Inman, D. J., and Park, G., 2005, “Comparison of Piezoelectric Energy Harvesting Devices for Recharging Batteries,” *J. Intell. Mater. Syst. Struct.*, **16**(10), pp. 799–807.
- [7] Zhu, D., Tudor, M. J., and Beeby, S. P., 2009, “Strategies for Increasing the Operating Frequency Range of Vibration Energy Harvesters: A Review,” *Meas. Sci. Technol.*, **21**(2), p. 022001.
- [8] Ferrari, M., Ferrari, V., Guizzetti, M., Marioli, D., and Taroni, A., 2008, “Piezoelectric Multifrequency Energy Converter for Power Harvesting in Autonomous Microsystems,” *Sens. Actuators A*, **142**(1), pp. 329–335.
- [9] Cornwell, P., Goethal, J., Kowko, J., and Damianakis, M., 2005, “Enhancing Power Harvesting Using a Tuned Auxiliary Structure,” *J. Intell. Mater. Syst. Struct.*, **16**(10), pp. 825–834.
- [10] Stanton, S. C., McGehee, C. C., and Mann, B. P., 2010, “Nonlinear Dynamics for Broadband Energy Harvesting: Investigation of a Bistable Piezoelectric Inertial Generator,” *Phys. D*, **239**(10), pp. 640–653.
- [11] Leland, E. S., and Wright, P. K., 2006, “Resonance Tuning of Piezoelectric Vibration Energy Scavenging Generators Using Compressive Axial Preload,” *Smart Mater. Struct.*, **15**(5), pp. 1413–1420.
- [12] Cheng, Y., Wu, N., and Wang, Q., 2017, “An Efficient Piezoelectric Energy Harvester With Frequency Self-Tuning,” *J. Sound Vib.*, **396**, pp. 69–82.
- [13] Peters, C., Maurath, D., Schock, W., Mezger, F., and Manoli, Y., 2009, “A Closed-Loop Wide-Range Tunable Mechanical Resonator for Energy Harvesting Systems,” *J. Micromech. Microeng.*, **19**(9), p. 094004.
- [14] Wu, X., Lin, J., Kato, S., Zhang, K., Ren, T., and Liu, L., 2008, “A Frequency Adjustable Vibration Energy Harvester,” *PowerMEMS*, Sendai, Japan, Nov. 9–12, pp. 245–248.
- [15] Challa, V. R., Prasad, M., Shi, Y., and Fisher, F. T., 2008, “A Vibration Energy Harvesting Device With Bidirectional Resonance Frequency Tunability,” *Smart Mater. Struct.*, **17**(1), p. 015035.
- [16] Roundy, S., and Zhang, Y., 2005, “Toward Self-Tuning Adaptive Vibration-Based Microgenerators,” *Proc. SPIE*, **5649**, pp. 373–385.
- [17] Nayfeh, A., Balachandran, B., Colbert, M., and Nayfeh, M., 1989, “An Experimental Investigation of Complicated Responses of a Two-Degree-of-Freedom Structure,” *ASME J. Appl. Mech.*, **56**(4), pp. 960–967.
- [18] Cao, D.-X., Zhang, W., and Yao, M.-H., 2010, “Analytical and Experimental Studies on Nonlinear Characteristics of an L-Shape Beam Structure,” *Acta Mech. Sin.*, **26**(6), pp. 967–976.
- [19] Zhang, W., Hu, W., Cao, D., and Yao, M., 2016, “Vibration Frequencies and Modes of a Z-Shaped Beam With Variable Folding Angles,” *ASME J. Vib. Acoust.*, **138**(4), p. 041004.
- [20] Bhaskar, K., and Pydah, A., 2014, “An Elasticity Approach for Simply-Supported Isotropic and Orthotropic Stiffened Plates,” *Int. J. Mech. Sci.*, **89**, pp. 21–30.
- [21] Pydah, A., and Bhaskar, K., 2015, “Accurate Discrete Modelling of Stiffened Isotropic and Orthotropic Rectangular Plates,” *Thin-Walled Struct.*, **97**, pp. 266–278.
- [22] Pydah, A., and Bhaskar, K., 2016, “An Accurate Discrete Model for Web-Core Sandwich Plates,” *J. Sandwich Struct. Mater.*, **18**(4), pp. 474–500.

- [23] Pydah, A., and Bhaskar, K., 2017, "Accurate Analytical Solutions for Shear-Deformable Web-Core Sandwich Plates," *J. Sandwich Struct. Mater.*, **19**(5), pp. 616–643.
- [24] Pydah, A., and Batra, R., 2018, "Analytical Solution for Cylindrical Bending of Two-Layered Corrugated and Webcore Sandwich Panels," *Thin-Walled Struct.*, **123**, pp. 509–519.
- [25] ABAQUS, 2014, "6.14 Documentation," Dassault Systèmes Simulia Corporation, Providence, RI.
- [26] Liew, K., Hung, K., and Lim, M., 1995, "Three-Dimensional Vibration of Rectangular Plates: Effects of Thickness and Edge Constraints," *J. Sound Vib.*, **182**(5), pp. 709–727.
- [27] Batra, R., and Aimmanee, S., 2003, "Missing Frequencies in Previous Exact Solutions of Free Vibrations of Simply Supported Rectangular Plates," *J. Sound Vib.*, **265**(4), pp. 887–896.
- [28] Qian, L., Batra, R., and Chen, L., 2003, "Free and Forced Vibrations of Thick Rectangular Plates Using Higher-Order Shear and Normal Deformable Plate Theory and Meshless Petrov-Galerkin (MLPG) Method," *Comput. Model. Eng. Sci.*, **4**(5), pp. 519–534.
- [29] Batra, R., and Aimmanee, S., 2005, "Vibrations of Thick Isotropic Plates With Higher Order Shear and Normal Deformable Plate Theories," *Comput. Struct.*, **83**(12–13), pp. 934–955.
- [30] Batra, R., Liang, X., and Yang, J., 1996, "Shape Control of Vibrating Simply Supported Rectangular Plates," *AIAA J.*, **34**(1), pp. 116–122.
- [31] Vel, S. S., and Batra, R., 2001, "Analysis of Piezoelectric Bimorphs and Plates With Segmented Actuators," *Thin-Walled Struct.*, **39**(1), pp. 23–44.
- [32] Ghosh, K., and Batra, R. C., 1995, "Shape Control of Plates Using Piezoceramic Elements," *AIAA J.*, **33**(7), pp. 1354–1357.